

Digital Control of Magnetic Bearings in a Cryogenic Cooler

J. Feeley, A. Law and F. Lind
Department of Electrical Engineering
University of Idaho
Moscow, Idaho 83843

1 Introduction

This paper describes the design of a digital control system for control of magnetic bearings used in a spaceborne cryogenic cooler. The cooler was developed by Philips Laboratories for the NASA Goddard Space Flight Center and is described in detail in Reference 1. Six magnetic bearing assemblies are used to levitate the piston, displacer, and counter-balance of the cooler. The piston and displacer are driven by linear motors in accordance with Stirling cycle thermodynamic principles to produce the desired cooling effect. The counter-balance is driven by a third linear motor to cancel motion induced forces that would otherwise be transmitted to the spacecraft.

An analog control system is currently used for bearing control. The purpose of this project is to investigate the possibilities for improved performance using digital control. Areas for potential improvement include transient and steady state control characteristics, robustness, reliability, adaptability, alternate control modes, size, weight, and cost. The present control system is targeted for the Intel 80196 microcontroller family. The eventual introduction of Application Specific Integrated Circuit (ASIC) technology to this problem may produce a unique and elegant solution both here and in related industrial problems.

2 System Description

The long life and tight clearance requirements of the NASA cooler motivated the choice of frictionless magnetic bearings to magnetically levitate the piston, displacer, and counter-balance shafts. A schematic side view of a typical magnetic bearing assembly is shown in Figure 1. It shows the principal system components for vertical position control and illustrates their relationship within the overall magnetic bearing system. The optical sensors measure the shaft position relative to the housing. Dual sensors and signal conditioning circuitry are used to produce a highly accurate position signal for the system controller. The controller responds to the difference between the desired and actual positions and sends an output signal to a voltage amplifier. The amplifier adjusts the voltage applied to the bearing coil and produces an electromagnetic field between the pole pieces to change the vertical force applied to the shaft. The force moves the shaft to maintain the desired clearance between the shaft and the housing. Operation of the horizontal bearing control system is similar.

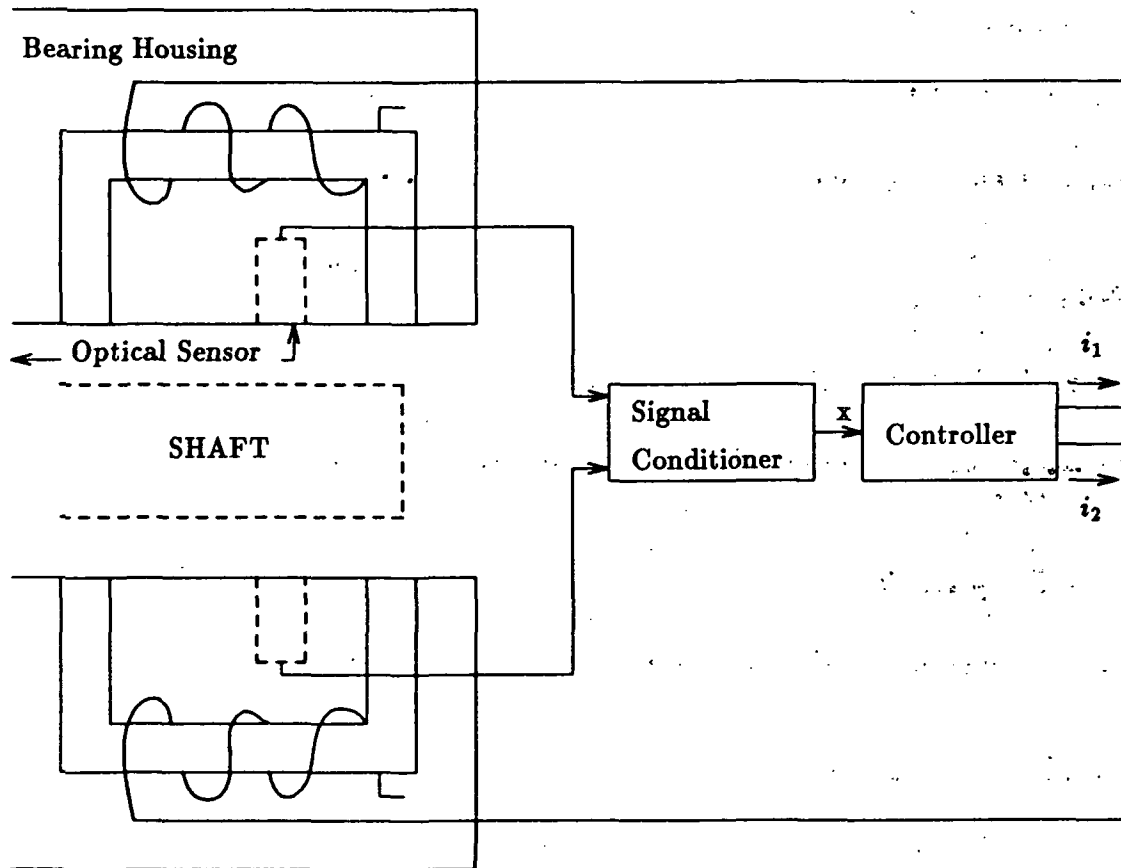


Figure 1: Typical magnetic bearing assembly.

3 Mathematical Models

Traditional control system design is based on a mathematical model of the system to be controlled. Relatively simple, linear, low order models are sought because of the availability of linear design tools and the insight and understanding provided by simple models. Once a candidate controller has been designed using linear methods, its performance is checked in a detailed nonlinear computer simulation of the closed loop system. Several iterative steps between linear system design and nonlinear simulation analysis usually produce an acceptable controller. In this section mathematical models are developed for the principal components in the magnetic bearing system.

3.1 Magnetic Bearing and Levitated Shaft

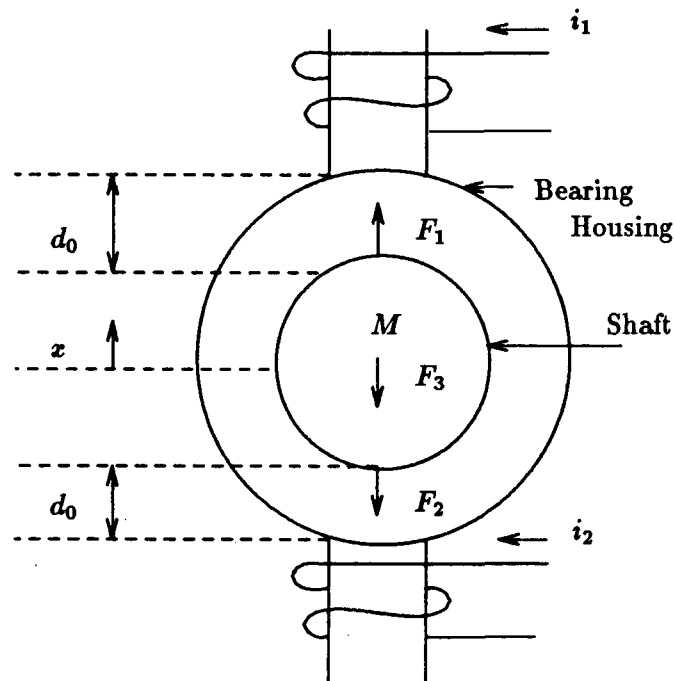


Figure 2: Free body diagram of levitated shaft

A free body diagram of one end of a levitated shaft is shown in Figure 2. The forces F_1 and F_2 are proportional to squares of the coil currents i_1 and i_2 in the respective pole piece coils and inversely proportional to the squares of the distances between the shaft and the pole pieces. F_3 is a viscous damping force due to the motion of the shaft through the helium working fluid. The vertical acceleration of the shaft is given by

$$\frac{d^2 x(t)}{dt^2} = \frac{1}{m}(F_1 - F_2 - F_3) \quad (1)$$

Substituting for the forces in terms of more basic variables gives

$$\frac{d^2 x(t)}{dt^2} = \frac{K_b}{m} \left[\frac{(i_0 + i)^2 (d_0 + x)^2 - (i_0 - i)^2 (d_0 - x)^2}{(d_0 - x)^2 (d_0 + x)^2} \right] - \frac{B}{m} \frac{dx(t)}{dt} \quad (2)$$

where K_b is the bearing constant of proportionality, m is the effective mass of the shaft supported by the bearing, i_0 is a constant bias current, i is the adjustable part of the current used for dynamic control, d_0 is the nominal bearing gap, x is the position of the bearing, and B is a viscous damping coefficient. Expanding Equation 2 in a Taylor series about the point $i = 0$, $x = 0$ yields the linear expression

$$\frac{d^2 x(t)}{dt^2} + K_1 \frac{dx(t)}{dt} - K_2 x(t) = K_3 i(t) \quad (3)$$

where the following definitions have been made:

$$\begin{aligned} K_1 &= \frac{B}{m} \\ K_2 &= \frac{4K_b i_0^2}{m d_0^3} \\ K_3 &= \frac{4K_b i_0}{m d_0^2} \\ K_b &= \frac{K_{eff} d_0^3}{4 i_0^2} \end{aligned}$$

and K_{eff} is the bearing stiffness under static conditions.

3.2 Bearing Actuator

A circuit model of the bearing actuator coils and pole pieces is shown in Figure 3.

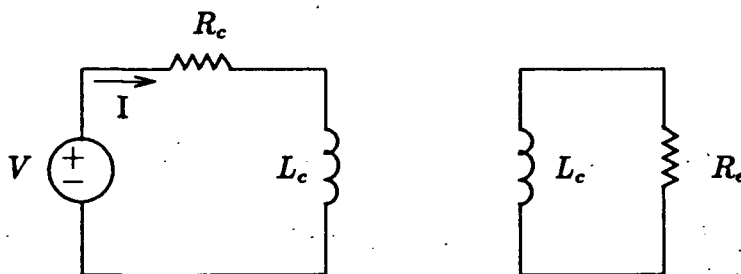


Figure 3: Circuit model of actuator coil

The circuit consists of a primary loop with a voltage source driving current through the equivalent resistance and inductance of the actuator coil. A secondary circuit consisting of a resistor and inductor in series is used to model the eddy currents set up in the actuator's pole piece.

The differential equation relating the actuator voltage and current is

$$\frac{d^2 i(t)}{dt^2} + K_4 \frac{di(t)}{dt} + K_5 i(t) = K_6 \frac{dv(t)}{dt} + K_7 v(t) \quad (4)$$

where the constants are defined as:

$$K_4 = \frac{L_c R_e + L_e R_c}{2L_c L_e}$$

$$K_5 = \frac{R_c R_e}{2L_c L_e}$$

$$K_6 = \frac{1}{2L_c}$$

$$K_7 = \frac{R_e}{2L_c L_e}$$

3.3 Optical Sensor

The dynamics of the optical sensor and its signal conditioning circuitry are very fast with respect to other components in the bearing system and for the purposes of control system design can be considered instantaneous. Noise and other sources of measurement error are small so that the position measurement is assumed to be perfect.

4 Control System Design

The design of a magnetic bearing control system is challenging for a number of reasons. The first, and most fundamental, is that the open loop system is unstable. This is obvious from the model equations and is due to the fact that the magnetic force of attraction on the shaft increases as the bearing gap decreases. Without active control, therefore, the shaft moves inexorably toward the bearing housing. Second, two stable but slow poles exacerbate the the instability by causing additional low frequency phase lag. The combination of these two factors causes traditional series compensators such as proportional- integral-derivative (PID), lead, lag, and lag-lead to fail as viable controllers. Additional control problems arise from the nonlinear system dynamics and the uncertain validity of the system model and its parameter values.

Nevertheless, there are a number of design tools that can be brought to bear on the problem. Even though the design objective is a digital controller, it is good practice to first design a corresponding analog controller. Since the sampling inherent with digital control inevitably degrades system performance the analog controller can serve as a useful benchmark. It is also possible, and this approach will be followed in this preliminary design study, to develop the digital controller from the analog controller by an appropriate mapping from continuous time to discrete time [2].

4.1 Design of Analog Controller

A particularly effective and widely used analog design method is the root locus technique of Evans. This method is especially appropriate in this problem because the open loop system is unstable and the sinusoidal steady state methods of Nyquist and Bode, while still applicable, require special care when used on non-minimum phase systems. So-called modern methods based on a state variable problem formulation and direct digital design techniques are also available and are being investigated. Regardless of what method is used, however, the resulting implementations are often surprisingly similar.

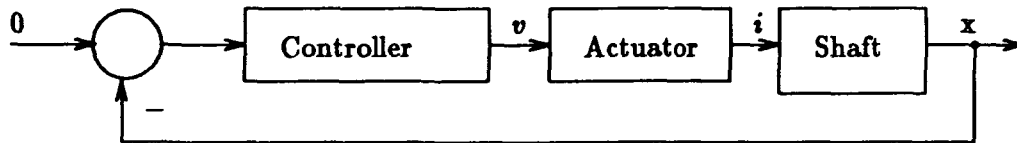


Figure 4: Block diagram of magnetic bearing system

Figure 4. is a block diagram of the closed loop magnetic bearing system and makes the choice of series compensation control explicit. The design procedure is best illustrated by example. Equations 3 and 4 are rewritten below using the numerical values obtained from Reference 1. The shaft equation is

$$\frac{d^2x(t)}{dt^2} + .0128 \frac{dx(t)}{dt} - 44x(t) = 11,940 i(t) \quad (5)$$

and the coil equation is

$$\frac{d^2i(t)}{dt^2} + 764.7 \frac{di(t)}{dt} + 11,460 i(t) = .7143 \frac{dv(t)}{dt} + 1082 v(t) \quad (6)$$

The range of coefficients in these equations suggests time scaling to produce a factor of 100 slowdown to facilitate design and analysis. Replacing t with $100/\tau$ in Equations 5 and 6 produces the time scaled equations for the shaft

$$\frac{d^2x(\tau)}{d\tau^2} + .00218 \frac{dx(\tau)}{d\tau} - .0044x(\tau) = 1.194i(\tau) \quad (7)$$

and the coil

$$\frac{di^2(\tau)}{d\tau^2} + 7.647 \frac{di(\tau)}{d\tau} + 1.146 i(\tau) = .007143 \frac{dv(\tau)}{d\tau} + .1082 v(\tau) \quad (8)$$

Taking Laplace transforms yields the shaft transfer function

$$\frac{X(S)}{I(S)} = \frac{1.194}{(S + .067)(S - .0657)} \quad (9)$$

and the coil transfer function

$$\frac{I(S)}{V(S)} = \frac{.007143(S + 15.15)}{(S - .06)(S + .07)(S + .15)(S + 7.5)} \quad (10)$$

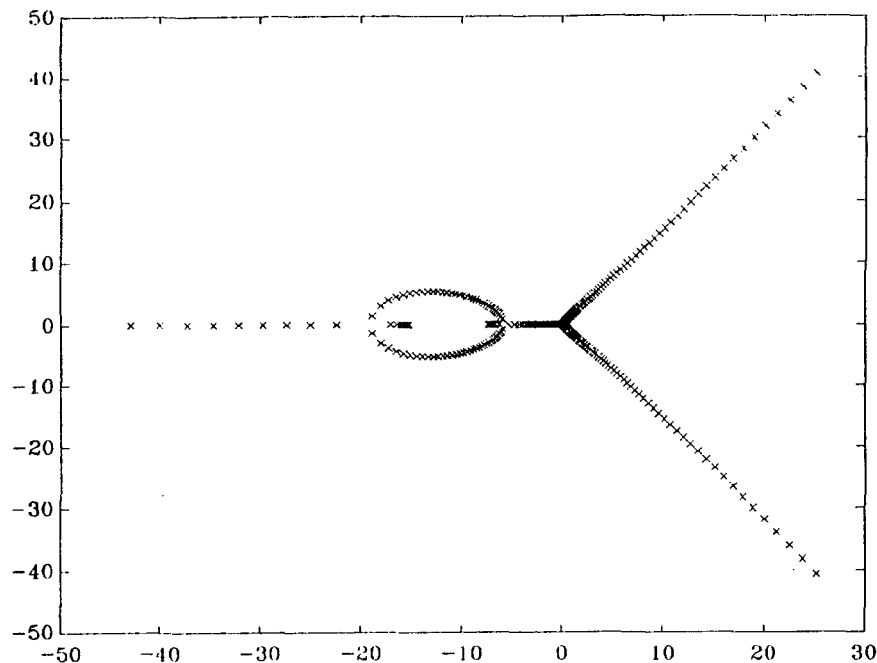


Figure 5: Root locus (scaled for 100:1 slowdown) of the uncompensated magnetic bearing

Cascading these two transfer functions produces the plant transfer function

$$G_p(S) \equiv \frac{X(S)}{V(S)} = \frac{.008(S + 15)}{(S - .06)(S + .07)(S + .15)(S + 7.5)} \quad (11)$$

where numerical values have been rounded for convenience.

The inherent instability of the plant is shown in the root locus of Figure 5 as a proportional gain factor varies from .001 to 10,000. The root locus clearly shows that the uncompensated plant is unstable for all values of gain. The pole-zero pattern and root locus plot reveal the essence of the control problem. The poles at -.07 and -.15 must be canceled, or nearly so, with compensating zeros to allow the unstable root to migrate into the left half plane. The compensator zeros may then be balanced with poles farther into the left half plane for noise suppression and to ensure a causal digital controller. Fast finite zeros may also be added further to the left of the new poles to aid in steady state error reduction.

A candidate controller with a double lead-lag characteristic meeting these requirements is given by

$$G_C(S) = K_C \left[\frac{(S + .1)(S + 100)}{(S + 10)^2} \right]^2 \quad (12)$$

The root locus of the compensated system is shown in Figure 6 as the controller gain varies from 1.25 to 1250.

The locus of the closed loop system roots shows a region of stable operation for controller gains between 6.25 and 250. Setting the controller gain to 62.5 yields a damping ratio from the dominant second order poles of about .78 which should produce fast step

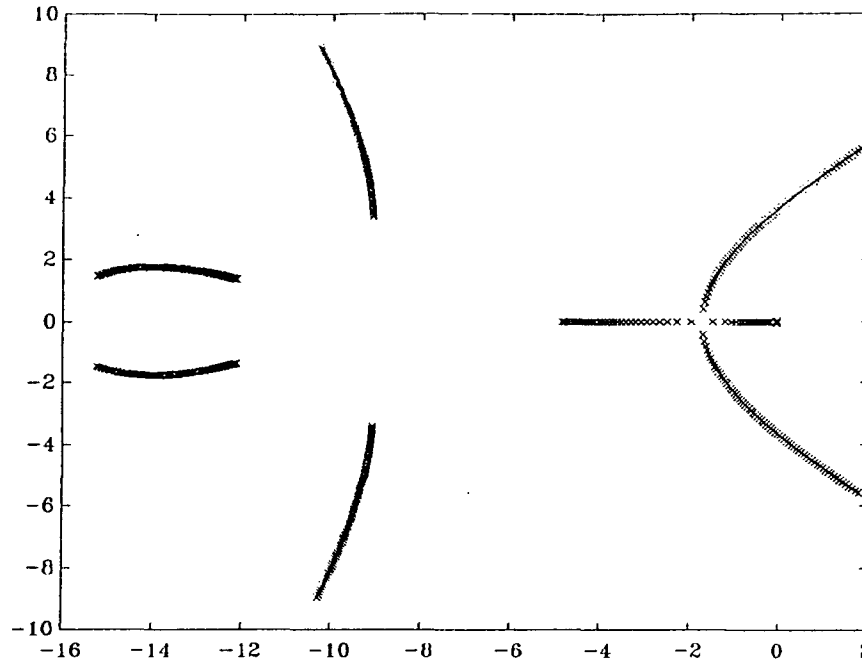


Figure 6: Root locus (scaled for 100:1 slowdown) of double lead-lag compensated system

response with less than 5% overshoot. This setting also produces reasonable robustness to gain variations allowing for a factor of 10 decrease and a factor of 4 increase before stability bounds are reached. The relative steady state error with this compensator and a gain of 62.5 is less than 7% or, about 1.3 microns for a nominal 19 micron gap. Steady state error could readily be reduced to less than 1 micron by increasing the gain to about 82.7 with little degradation of transient performance.

The response of the controlled system with a compensator gain of 62.5 to a unit step input is shown in Figure 7 and verifies transient performance and steady state error approximations. Bode plots of log magnitude and phase versus log frequency for the compensated open loop system with the same controller gain are shown in Figure 8.

They illustrate the care required in interpreting these plots for non-minimum phase systems. Note that while the plots indicate nearly 180 deg of phase shift at low frequencies where the open loop gain is greater than 1, this is due to the right half plane pole. Also note the time and frequency scale factors on the plots.

4.2 Design of Digital Controller

Given an analog controller design as embodied in the transfer function of Equation (12) there are a number of methods of developing an equivalent digital controller. The basic procedure in each approach is to select an appropriate mapping to convert the Laplace transform transfer function to an equivalent Z transform transfer function. Taking the inverse Z transform of this transfer function produces a difference equation that determines the digital control algorithm.

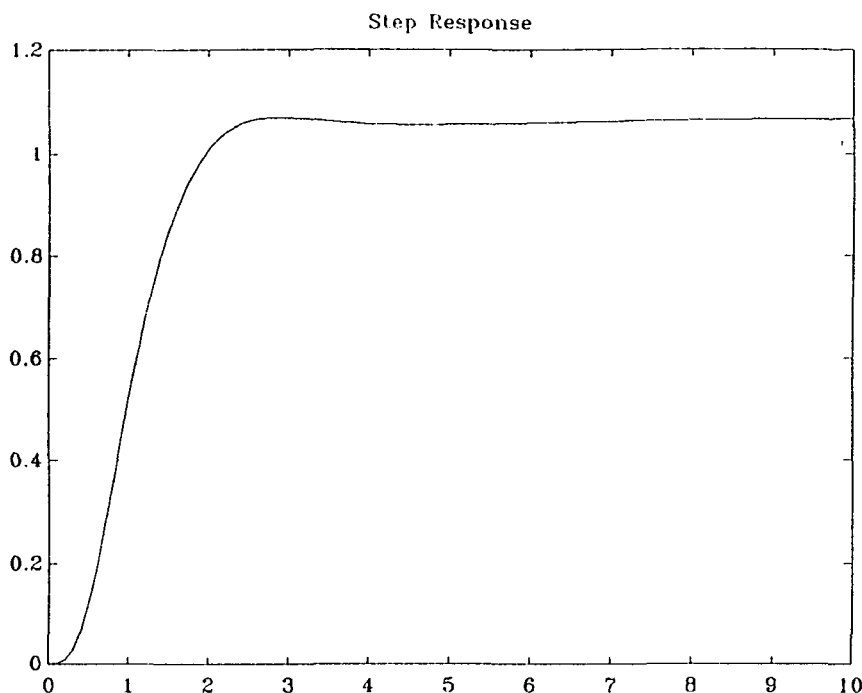


Figure 7: Step response (scaled for 100:1 slowdown) of compensated system

One commonly used method based on trapezoidal integration, and often referred to as the Tustin or bi-linear transformation, uses the substitution

$$S = \frac{2z - 1}{Tz + 1} \quad (13)$$

This mapping introduces the parameter T , the sampling interval. Experience has shown [2] that if the sampling frequency is 20 or more times higher than the highest frequency present in the system the digital controller behaves similarly to the equivalent analog controller and justifies the analog emulation design method. Figure 8 indicates that the bearing system bandwidth is approximately 100 rad/sec or about 16 Hertz. Choosing a sampling frequency of 500 Hertz, over 30 times the system bandwidth, should give good performance. This sampling rate corresponds to a sampling period of 2 msec and thus imposes an upper limit on the total time required to perform the analog to digital conversion, the digital control calculation, and digital to analog conversion in the digital controller.

Applying the Tustin transformation to the analog controller transfer function give the digital transfer function

$$G_c(z) = 62.5 \left[\frac{(1010z - 990)(11,000z + 9000)}{(2000z)^2} \right]^2 \quad (14)$$

Taking the inverse Z transform gives the controller difference equation relating the controller input $y(k)$ to the controller output $u(k)$

$$y(k) = 62.5 [7.714u(k) - 2.5u(k-1) - 12.17u(k-2) + 2u(k-3) + 4.962u(k-4)] \quad (15)$$

7.2.10

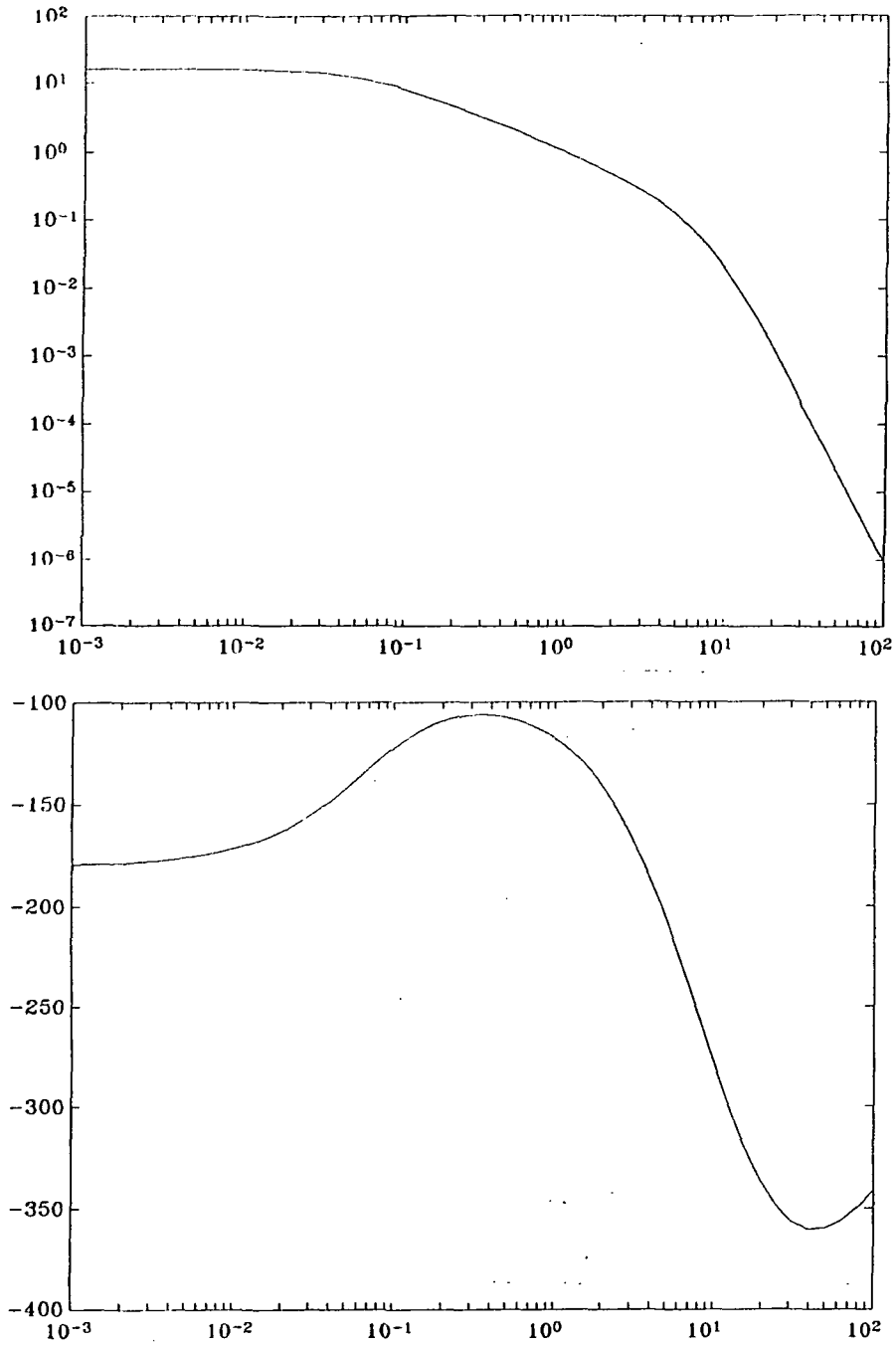


Figure 8: Bode magnitude and phase plots (scaled for 100:1 slowdown) of compensated open loop transfer function

C-5.

Different algebraic approaches will produce different forms for the controller difference equation that may have some timing or scaling advantages, but Equation (15) will serve as a suitable point of departure for further studies. It should also be noted that since the controller transfer function is merely a proper (as opposed to strictly proper) rational function, a controller output $y(k)$ is required at the same instant the latest measurement $u(k)$ is received. This non-causal characteristic can be ameliorated somewhat by appropriate sequencing of computations and data output in the control algorithm.

5 Conclusions and Future Work

A simple nonlinear magnetic bearing model was developed from first principles. Model parameters have been evaluated from readily available data and the model appears consistent with reported experimental data. A double lead-lag analog control system based on the linearized model equations was designed. The controller is effective in stabilizing the unstable plant, providing good transient response, and acceptable steady state error. An equivalent digital controller was developed from the analog controller using Tustin's transformation. The selected sampling rate, 500 Hertz, is over 30 times the highest system frequency and should cause the digital controller to perform nearly as well as the analog controller.

Work is currently proceeding on several fronts. A detailed nonlinear simulation of the magnetic bearing and its controller is being developed. This will be a useful tool for evaluating candidate controllers and sampling rates. A microcontroller based on the Intel 80196 family is being developed. It will be interfaced with an analog computer simulation of the magnetic bearing for real time testing. Candidate architectures for an ASIC real time controller chip are being evaluated. Advanced robust control design methods are being tested for use in direct design of a robust digital controller. Adaptive performance feedback and fuzzy control methods are also being investigated to form the foundation of an adaptive bearing controller.

References

- [1] F. Stolfi et. al., "Design and fabrication of a long-life Stirling cycle cooler for space application," Philips Laboratories report, March, 1983.
- [2] G.F. Franklin, J.D. Powell, and M.L. Workman, "Digital control of dynamic systems," Addison-Wesley, 1990.